Key innate immune components controlling intracellular infection

Benard, E.L.

Chapter 6

The macrophage-expressed perforins Mpeg1 and Mpeg1.2 have anti-bacterial function in zebrafish

Erica L. Benard[1], Peter I. Racz[1], Julien Rougeot[1], Alexander E. Nezhinsky[2], Fons J. Verbeek[2], Herman P. Spaink[1], Annemarie H. Meijer[1]

[1]Institute of Biology Leiden, Leiden University
[2]Leiden Institute for Advanced Computer Science, Leiden University

Journal of Innate Immunity, In press

Abstract

Macrophage expressed gene 1 (*MPEG1*) encodes an evolutionary conserved protein with a predicted Membrane Attack Complex/Perforin domain associated with host defence against invading pathogens. In vertebrates, MPEG1/Perforin-2 is an integral membrane protein of macrophages, suspected to be involved in killing of intracellular bacteria by pore-forming activity. Zebrafish have three copies of *MPEG1*, two of which are expressed in macrophages, whereas the third could be a pseudogene. The *mpeg1* and *mpeg1.2* genes show differential regulation during infection of zebrafish embryos with the bacterial pathogens, *Mycobacterium marinum* and *Salmonella typhimurium*. While *mpeg1* is down-regulated during infection with both pathogens, *mpeg1.2* is infection inducible. Up-regulation of *mpeg1.2* is partially dependent on the presence of functional Mpeg1, and requires the Toll-like receptor adaptor molecule MyD88 and transcription factor NFκB. Knockdown of *mpeg1* alters the immune response to *M. marinum* infection and results in increased bacterial burden. In *S. typhimurium* infection, both *mpeg1* and *mpeg1.2* knockdown increase bacterial burdens, but *mpeg1* morphants show increased survival time. The combined results of these two *in vivo* infection models support the anti-bacterial function of the MPEG1/Perforin-2 family and indicate that the intricate cross-regulation of the two *mpeg1* copies aids the zebrafish host in combatting infection of various pathogens.

Introduction

Membrane Attack Complex/Perforin (MACPF) proteins belong to a large superfamily of pore forming molecules present in almost all living organisms [1, 2]. In vertebrates, MACPF proteins perform crucial roles in immune defence against both extracellular and intracellular infections [3, 4]. The MACPF domain is present in the components of the terminal complement pathway (C6, C7, C8, and C9), which form the membrane attack complex (MAC) targeting gram-negative bacteria and certain pathogenic parasites directly by forming pores on their cell membranes [1]. The MACPF domain is also present in the perforins released by cytotoxic T lymphocytes and natural killer cells, which create pores in the plasma membranes of infected and transformed host cells, allowing the entry of cytolytic proteins [4].

In addition to the complement proteins and the perforins, there is another MACPF domain-containing membrane protein involved in the immune system, named Macrophage expressed gene 1 (MPEG1) or Perforin-2 [3]. *MPEG1* was first identified as a macrophage-specific gene in human and mice, but how it contributes mechanistically to macrophage defence remains to be elucidated [3, 5]. Homologs of *MPEG1* are found in marine metazoans, such as the sea sponge [6], the pacific oyster [7], and abalone shellfish [8], and evolutionary reconstruction suggests that an ancestral *MPEG1* gene gave rise to the vertebrate perforin genes [9]. Expression of *MPEG1* homologs in the invertebrates is up-

regulated by viral and bacterial infections or by exposure to bacterial lipopolysaccharide (LPS) [6-8]. Furthermore, recombinant sea sponge Mpeg has been shown to inhibit bacterial growth *in vitro* [6]. In mice, *Mpeg1* (also named *Perforin-2*) is up-regulated during prion infection and its expression could be induced in primary mouse embryonic fibroblasts by several types of bacterial infections [10, 11]. Mouse embryonic fibroblasts rapidly induce expression of *Mpeg1* in response to infection with *Mycobacterium smegmatis*, and these fibroblasts lose their ability to kill this non-pathogenic mycobacterium species when *Mpeg1* is knocked down with siRNA [11]. Furthermore, this study showed that *M. smegmatis* bacteria are sensitive to the bacteriolytic activity of lysozyme when they are recovered from *Mpeg1*-expressing fibroblasts but not when they are recovered from *Mpeg1*-deficient cells, suggesting physical attack of the bacterial membrane by the MACPF domain of Mpeg1 [11]. It has also been shown that Mpeg1 restricts growth of *Chlamydia trachomatis* in macrophages, while studies in HeLa cells suggest that chlamydiae are protected from Mpeg1-mediated killing in epithelial cells by prevention of *Mpeg1* transcription [12]. Following ectopic expression of *Mpeg1* in HeLa cells, the protein concentrated around the chlamydia-containing vacuoles and inhibited chlamydial growth. It has been proposed that the MACPF domain of Mpeg1 is oriented inside membrane vesicles and that upon bacterial infection these vesicles traffic and fuse with bacteria-containing endosomes to mediate bacterial killing by pore formation[3].

The zebrafish genome contains an *mpeg1* gene that like its human and murine counterpart is expressed by macrophages and encodes a protein with the conserved MACPF domain as well as the characteristic transmembrane region [13, 14]. There are several advantages for using zebrafish as a model to study host-pathogen interactions. Firstly, the free-living zebrafish embryos and early larval stages are optically transparent and *in vivo* visualization of infectious disease processes is facilitated by various transgenic lines, including reporter lines using the *mpeg1* promoter to drive fluorescent protein expression in macrophages [14]. Secondly, genetic approaches are easily applicable, such as the efficient inactivation of gene functions achieved by injection of antisense morpholino oligonucleotides. Thirdly, it is possible to study the innate immune response in the absence of an adaptive immune contribution. Already at 1 day post fertilisation (dpf) the innate immune system of the zebrafish embryo is capable of defence against microbial infections [15], while the adaptive immune system does not mature before three weeks of age [16]. Differentiated myeloid cells of the innate immune system are able to phagocytose apoptotic cell corpses [15] and adhere and phagocytose bacteria injected into the blood [15, 17, 18]. These properties led to the development of zebrafish infection models for a wide variety of pathogens [19].

In this study, we used well-established zebrafish embryo models for *Mycobacterium marinum* and *Salmonella enterica* serovar Typhimurium (*S. typhimurium*) infections to investigate the function of *mpeg1* and one of its paralogues named *mpeg1.2*. We show that these two MPEG1 homologues are differentially regulated during infection and provide *in vivo* evidence for the function of both genes in anti-bacterial defence.

Materials and methods

Zebrafish lines and handling of embryos

Zebrafish were handled in compliance with the local animal welfare regulations and were maintained according to standard protocols (zfin.org). The culture was approved by the local animal welfare committee (DEC) of the University of Leiden and all protocols adhered to the international guidelines specified by the EU Animal Protection Directive 2010/63/EU. Adult zebrafish were not sacrificed for this study. All experiments in this study were performed on embryos/larvae before the free-feeding stage and did not fall under animal experimentation law according to the EU Animal Protection Directive 2010/63/EU. Zebrafish lines used in this study included AB/TL, *myd88*^{hu3568} [20], *Tg(mpx:gfp)*^{i114} [21], *Tg(mpeg1:EGFP)*^{gl22} [14], and *Tg(mpeg1:mCherry-F)*^{UMSF001} [22]. Embryos were grown at 28.5-30°C in egg water (60 µg/ml Instant Ocean sea salts). For the duration of bacterial injections and imaging, embryos were kept under anaesthesia in egg water containing 200 µg/ml tricaine (Sigma-Aldrich). Embryos used for stereo fluorescence imaging were kept in egg water containing 0.003% 1-phenyl-2-thiourea (Sigma-Aldrich) to prevent melanisation.

Morpholino knockdown

Morpholino oligonucleotides (Gene Tools) were diluted to the desired concentration in 1x Danieau buffer (58 mM NaCl, 0.7 mM KCl, 0.4 mM $MgSO_4$, 0.6 mM $Ca(NO_3)_2$, 5.0 mM HEPES; pH 7.6) containing 1% phenol red (Sigma-Aldrich) and 1 ηL was injected into the yolk at the 1-2 cell stage using a Femtojet injector (Eppendorf). For knockdown of *mpeg1* or *mpeg1.2*, two morpholinos each were used, one targeting the exon 1-intron 1 splice junction (*mpeg1* Mo1: 5'ATTTTGTACTTACTTGAACCCGTGC3', 0.3 mM; *mpeg 1.2* Mo1: 5'ACTTTTCTGTCTTACCTGAACTCGT3', 0.1 mM), and the other targeting the intron 1-exon 2 splice junction (*mpeg1* Mo2: 5'GGTTACGGACCTGAGAAACAAATTT3', 0.1 mM; *mpeg 1.2* Mo2: 5'TGCGTACCTGAGAAGATAACACAAA3', 0.1 mM). For knockdown of *ptpn6* the splice junction morpholino 1 (*ptpn6* Mo1: 5'ACTCATTCCTTACCCGATGCGGAGC3') was used as described previously [23]. As a control, the standard control morpholino from Gene Tools was used at the same concentrations as the other morpholinos.

Chemical treatments

NFκB activation inhibitor (NAI, 50 nM, 4 hours total treatment, including 2 hours pre-treatment, Calbiochem, #481406) and copper sulphate ($CuSO_4$, 10 uM, 2 hours treatment) Merck, #1027910250) [24] were administered via the egg water. After copper sulphate treatment the embryos were briefly washed three times with egg water and fixed in 4% paraformaldehyde in PBS.

Infection experiments

Mycobacterium marinum infections were performed using the Mma20 strain expressing mCherry in a pSMT3 vector [25] or the M strain expressing GFP in a pMSP12 vector [26]. *M. marinum* was heat-killed by incubation in 80°C for 20 min and plated during injections to control for bacterial growth. *S. typhimurium* infections were performed using the *S. typhimurium* strain SL1027 and its isogenic LPS Ra mutant derivative SF1592, carrying the DsRed expression vector pGMDs3 [18], and *Staphylococcus epidermidis* infections were performed using strain O-47 [27]. Embryos were staged at 24 hpf by morphological criteria and manually dechorionated. Bacteria were prepared and injected into the blood circulation at 28 hpf, and PBS or 2% PVP was injected as a control [28]. The same conditions were used for injection of 1 nl of LPS from *S. typhimurium* dissolved in PBS (10 µg/ml, Sigma, #L6511). For *S. typhimurium* plating assays, groups of 5 infected embryos (150 cfu) were homogenised using a Bullet blender (Next advance) for 3 minutes, speed 4 with 5 1.0 mm Zirconium Oxide beads, density is 5.5g/cc and a dilutions series was plated at 1 and 16 hpi.

Fluorescence-activated cell sorting

Macrophages and neutrophils were isolated by FACS from 6 dpf *Tg(mpeg1:mCherry-F)*^{UMSF001} [22] and *Tg*(*mpx*:*egfp*)^{i114} [21] zebrafish larvae, respectively, and the RNA was extracted as described [13].

RNA isolation, cDNA synthesis, and expression analyses

Whole embryo RNA isolation, removal of residual genomic DNA, cDNA synthesis and quantitative RT-PCR (qPCR) analysis was performed as described in [29]. qPCR results were analysed using the ΔΔCt method. All reactions were performed as technical duplicates and data were normalised to the expression of peptidylprolyl isomerase A like (*ppial*) for whole embryo samples and to (*eif4*) for cells isolated by FACS. Primer sequences for *ppial* and *mpeg1* are described in [13], primer sequences for *mmp9* and *il1b* are described in [29], primer sequences for *mpeg1.2* were: FW: 5'TCAGGCCAATGTGAACGACA3'; REV: 5'GGTGACTCAGGAGTGCATGT3', and primer sequences for *eif4a1b* were: FW: 5'TTCAGAAACTCAGTACTAGCATACA3'; REV: 5'GTGACATCCAACACCTCTGC3'. Knockdown of mpeg1 with both morpholinos was verified by qPCR and to validate the knockdown of *mpeg1.2* with both morpholinos, the SuperScript® One-Step RT-PCR System (Invitrogen, #10928-034) was used with 50ng DNAse treated RNA template. RT-PCR primers for *mpeg1.2* Mo1 knockdown verification were FW: 5'CTGCGCAATTTAGACGTGGG3'; REV: 5'GACGTGTCGTTCACATTGGC3', and for Mo2 were FW: as Mo1 primer; REV: 5'TTAATGCCTGCGGATGCAGA3'. The following adjustments were made to the PCR settings: 59.4°C for 30 seconds for the annealing step of the PCR amplification with 40 cycles.

RNA for deep sequencing analysis was isolated using QIAzol lysis reagent and purified

using the Rneasy MinElute Cleanup kit (QIAGEN Benelux B.V., Venlo, Netherlands). RNA sequencing was performed as previously described [27]. Gene Expression Omnibus (GEO) database accession for RNASeq: GSE49188 and GSE54885.

Immunohistochemistry and enzyme histochemistry

For simultaneous identification of *S. typhimurium*, neutrophils and macrophages a combination of immuno-labelling and enzymatic staining was used. First a neutrophil specific staining for myeloperoxidase (mpx) activity was performed. This was achieved by fixing embryos in 4% PFA in 4 °C overnight, washing three times briefly in PBSTx (PBS with 0.05% Triton X100 (Sigma Aldrich)), washing briefly in amp diluent from the TSA Plus Fluorescein System kit (Perkin Elmer) and incubating in 1:50 of Fluorescein in amp diluent at 28 °C for 10 minutes. The embryos were then washed again three times in PBSTx and fixed in 4% PFA for 20 minutes at room temperature. Next, the embryos were immuno-labelled with an anti-*Salmonella* polyclonal antibody with an Alexa 568-conjugated secondary antibody as described [30]. Finally, total leukocytes were immuno-labelled with an L-plastin antibody and Alexa 633-conjugated secondary antibody [31]. Macrophages were identified as L-plastin-positive, mpx-negative cells.

Image analysis

Fluorescence images were taken with a Leica MZ16FA stereo fluorescence microscope equipped with a DFC420C digital colour camera. In *M. marinum* infection experiments, bacterial pixel counts were obtained with stereo fluorescence images and analysed using dedicated pixel quantification software [32]. Each image contains two channels: bright field and fluorescence. Image recognition software identifies the location of each embryo (each image can contain up to 3 embryos) and links the outline and orientation per embryo in the bright field channel to the fluorescence channel. Each fluorescent pixel is quantified and allocated to a location in the embryo (background is determined by a non-infected control) and the software provides the value of total amount of fluorescent pixels per embryo. This is done for all groups of embryos and the results are written to a comma-separated file for statistical analysis. Leukocyte counts were performed on a Zeiss AxioObserver confocal microscope with an EC PlnN 10x 0.3 NA objective and all other confocal images were taken on a Leica TCS SPE with HCX APO 40x 0.8 NA objective. Maximum intensity projections of merged channel confocal images were made in Fiji.

Statistical Analysis

Data (mean ± SEM) were analysed (Prism 5.0, GraphPad Software, San Diego, CA) using unpaired, two-tailed t-tests for comparisons between two groups and one-way ANOVA with Tukey's Multiple Comparison method as a post-hoc test for other data (*, $p<0.05$; **, $p<0.01$; ***, $p<0.001$). Statistical significance in survival curves was determined by a logrank test.

Results

The zebrafish genome contains a conserved family of *mpeg1* genes

The zebrafish *mpeg1* gene (Chromosome 8: ENSDARG00000055290) was previously described as a macrophage-specific marker [13 14]. Inspection of the zebrafish reference genome sequence showed that two paralogues of the *mpeg1* gene are present on the same chromosome (fig. 1A). In consultation with the zebrafish nomenclature committee (ZFIN) the three *mpeg1* genes have been named *mpeg1.1* (hereafter referred to as *mpeg1* for consistency with previous publications and nomenclature of derived transgenic lines), *mpeg1.2* (Chromosome 8: ENSDARG00000043093), and *mpeg1.3* (Chromosome 8: ENSDARG00000078569). All three of the predicted Mpeg1 proteins contain conserved regions also found in mouse and human MPEG1, including a signal peptide, a Membrane Attack Complex/Perforin (MACPF) domain, and a transmembrane region (fig. 1B). Amino acid alignment of Mpeg1 and Mpeg1.2 reveals that these domains are located in the same positions (supplementary fig. 1). The three zebrafish Mpeg1 isoforms show around 80-90% amino acid similarity (with ca. 60-70% identity) among each other and their similarity with murine and human MPEG1 (overall and within the MACPF domain) is around 70-80% (with between 43 and 50% identity) (supplementary table 1A, B).

The *mpeg1* promoter region has been successfully used to drive macrophage-specific expression in zebrafish transgenic reporter lines [14, 22]. We determined RNAseq profiles of macrophages isolated from 5 day old *Tg(mpeg1:mCherry-F)*^{UMSF001} zebrafish larvae by FACS and found expression of both *mpeg1* and *mpeg1.2* to be enriched in the fluorescent macrophage cell fraction compared to the fluorescent-negative background (data not shown). The macrophage-specific expression of these two genes was confirmed by qPCR analysis on the same cell fractions and their expression was not enriched in neutrophils sorted from *Tg*(*mpx*:*egfp*)^{i114} [21] transgenic larvae (fig. 1C+D). Expression of *mpeg1.3* was not observed in any of our RNAseq deep sequencing data sets of larval leukocyte populations or of different bacterial infection experiments in various embryonic, larval and adult stages, and it is well possible that this is a pseudogene. Therefore, we focussed this study on *mpeg1* and *mpeg1.2*.

Mpeg1 expressing macrophages participate in the formation of granuloma-like structures

The development of the *mpeg1*-driven transgenic lines has opened a new window of opportunity for detailed visualisation of host-pathogen interactions. We have previously shown that *mpeg1*-expressing macrophages are capable of phagocytosing both *S. typhimurium* and *M. marinum* bacteria [28]. The hallmark of infection with pathogenic mycobacteria is the clustering of infected macrophages into granuloma-like aggregates [17]. We used the *Tg(mpeg1:mCherry-F)*^{UMSF001} line to study the behaviour

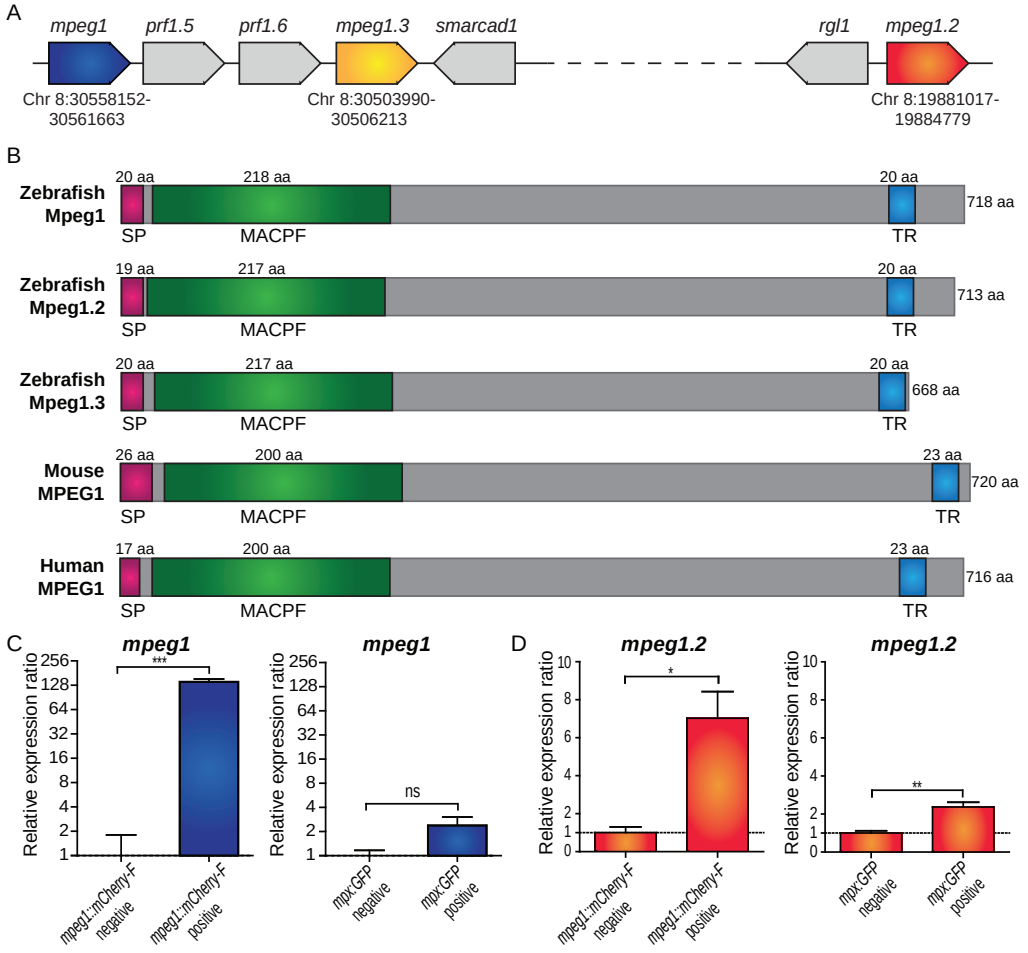

Figure 1. Zebrafish *mpeg1* genes encode proteins with conserved transmembrane and Membrane Attack Complex/Perforin domains and are expressed in macrophages. (A) Schematic representation of the region containing the genes *mpeg1*, *mpeg1.2* and *mpeg1.3* on zebrafish chromosome 8 (Chr 8). Coding direction of the genes is indicated by the pointed end and the exact location is indicated in digits below the gene. (B) Comparison of the predicted Mpeg1, Mpeg1.2, and Mpeg1.3 protein structures with murine and human MPEG1. The Signal Peptide (SP), Membrane Attack Complex/Perforin (MACPF), and Transmembrane Region (TR) are conserved domains detected by SMART analysis. (C-D) Expression of zebrafish *mpeg1* and *mpeg1.2* in (C) macrophages and (D) neutrophils. qPCR analysis was performed on RNA from fluorescence-positive cell fractions obtained by cell sorting of 6 dpf larvae of transgenic reporter lines for macrophages (mpeg1: *Tg(mpeg1:mCherry-F)*) and neutrophils (mpx: *Tg(mpx:EGFP)*). Expression was compared against the fluorescence-negative cell fraction of each transgenic line. Graphs show data combined of three biological replicates ((C) log2 scale).

of *mpeg1*-expressing macrophages during infection with GFP-expressing *M. marinum*. Imaging the same site of infection over a 0-5 days post infection (dpi) time course clearly showed that *mpeg1*-positive macrophages contribute to the formation of the tight granuloma-like structure (fig. 2). At 8 hours post infection (hpi) the majority of phagocytosed *M. marinum* bacteria were contained within *mpeg1*-positive cells. By 3 dpi *mpeg1*-positive infected cells had formed a compact centre of a growing granuloma-like aggregate, to which many uninfected *mpeg1*-macrophages were attracted. The *M. marinum*-containing *mpeg1*-positive cells showed a rounded morphology at this stage, while *mpeg1*-positive cells attracted to the border of granulomas showed a branched morphology similar to that of *mpeg1*-positive cells in uninfected embryos. At 4 dpi the granuloma structures had become more compact. At 5 dpi, cording of *M. marinum* was observed in granulomas indicative of extracellular growth, while less mCherry-fluorescent macrophages were present compared to 4 dpi, consistent with the occurrence of infected macrophage cell death at this stage [33]. The remaining mCherry-fluorescent cells all showed a rounded morphology, markedly different from the extensively branched morphology of mCherry-fluorescent macrophages in uninfected embryos (fig. 2A). While these data do not exclude the possible presence of other macrophage subpopulations, it shows that the majority of macrophages contributing to granuloma formation can be traced using the *mpeg1* marker.

Opposite regulation of *mpeg1* and *mpeg1.2* during infection

Analysis of the *Tg(mpeg1:mCherry-F)*^{UMSF001} reporter line indicated that the *mpeg1* promoter version driving the expression of mCherry in this transgenic line is active over the entire time course of *M. marinum* infection, from the 1 day old embryo up to the larval stage. However, in *S. typhimurium* infection of embryos we had previously observed that *mpeg1* expression is down-regulated [23, 29]. These observations prompted us to further investigate the regulation of *mpeg1* expression during different infections and compare this with the expression of the closely related *mpeg1.2* gene. First, we examined *mpeg1* and *mpeg1.2* expression by qPCR during a time course of *M. marinum* infection ranging from 2 hpi up to 5 dpi (fig. 3A). Within several hours after the intravenous injection of *M. marinum,* the expression level of *mpeg1* declined as compared to the mock-injected controls and this resulted in a significant down-regulation of approximately 3-fold at 8 hpi (fig. 3B). A similar trend, although not significant, was observed at 8 hpi in embryos infected with the attenuated *M. marinum* ΔRD1 strain (supplementary fig. 2A) as well as in embryos infected with heat-killed *M. marinum* (supplementary fig. 2B). This indicates that the *mpeg1* down-regulation response results from the presence of *M. marinum* and is independent of the virulence or viability of the bacteria. Between 1 to 3 dpi, the level of expression returned to control levels, but at 4 dpi a minor but significant down-regulation was observed again (fig. 3C). In contrast, expression of *mpeg1.2* was unaffected up to 3 dpi and was significantly up-regulated at 4 and 5 dpi (fig. 3C).

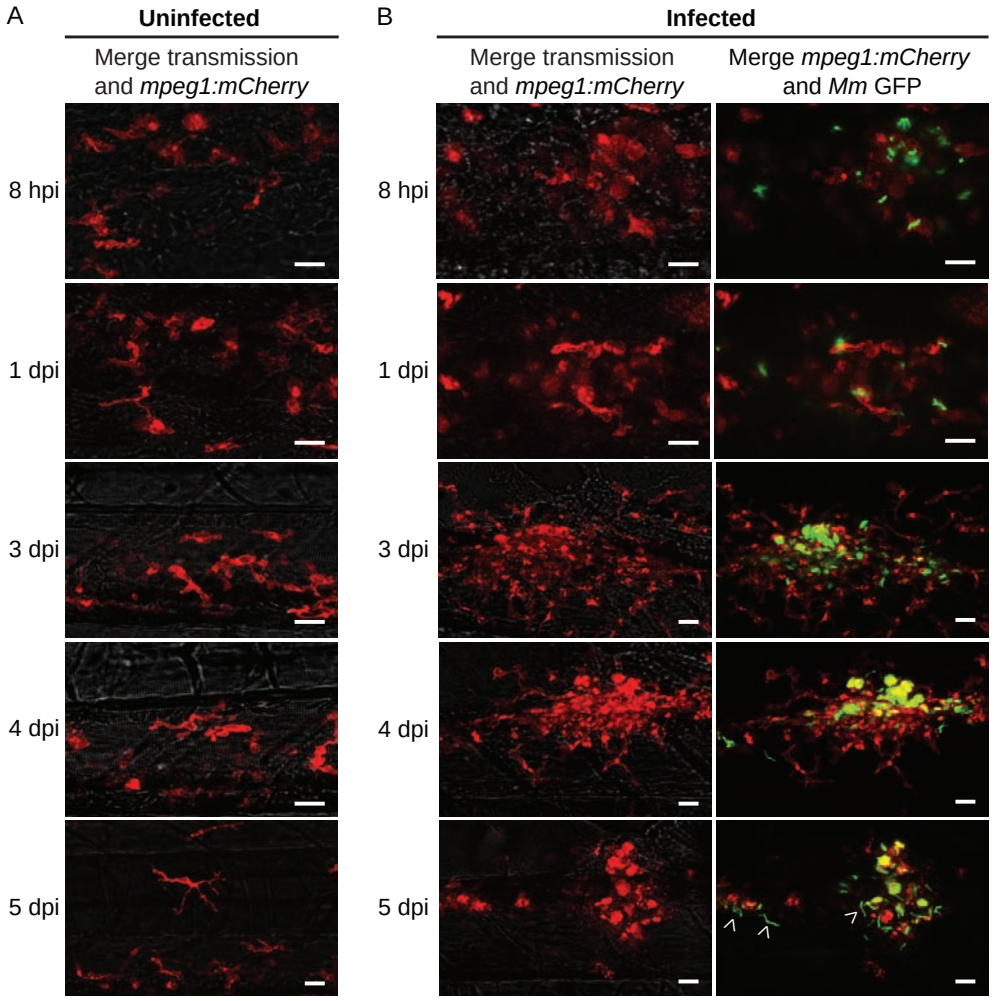

Figure 2. Tg(*mpeg1*)-positive macrophages are involved in formation of *M. marinum* granuloma-like aggregates. GFP-expressing *M. marinum* M-strain (150 cfu) bacterial infection in *Tg(mpeg1:mCherry-F)* zebrafish embryos. Confocal z-stack projections showing identical locations in the posterior region of the caudal haematopoietic tissue in (A) an uninfected embryo and (B) an infected embryo developing a granuloma-like aggregate (same infection site followed over time). Images were taken at 8 hours post injection (hpi), 1 dpi, 2 dpi (not shown), 3 dpi, 4 dpi and 5 dpi. Arrowheads indicate cording of *M. marinum*. Scale bar: 20 µm.

Next, we investigated if *mpeg1* and *mpeg1.2* were also differentially regulated during *S. typhimurium* infection. Intravenous *S. typhimurium* infection in zebrafish embryos is acute and lethal within one day [18]. We have previously reported a robust induction of pro-inflammatory gene expression at 8 hpi [23, 29] and therefore investigated *mpeg1* and *mpeg1.2* expression at this time point. While *mpeg1* showed approximately 4-fold down-regulation, *mpeg1.2* was up-regulated more than 10-fold (fig. 3D). The uninfected and *S. typhimurium* infected embryos at 8 hpi contained similar numbers

of macrophages (uninfected 54 ± 4.5 s.e.m., n=16 embryos; infected 51 ± 3.6 s.e.m., n = 15 embryos). Furthermore, as previously shown, expression of other markers for zebrafish embryonic macrophages, including *csf1r*, *cxcr3.2*, and *mfap4*, is unchanged at this time point of infection, indicating the specificity of the alterations in *mpeg1* and *mpeg1.2* expression [23]. Infection with an attenuated lipopolysaccharide (LPS) mutant of *S. typhimurium* (Ra) [18] also led to significant down-regulation of *mpeg1*, but *mpeg1.2* showed only a slight and non-significant up-regulation (supplementary fig. 2C). We also observed down-regulation of *mpeg1* and up-regulation of *mpeg1.2* in infection models for *Staphylococcus epidermidis* (supplementary fig. 2D-E), indicating that the differential regulation of these genes is a more general phenomenon in response to bacterial infections.

The opposite regulation of *mpeg1* and *mpeg1.2* raised the question if these two genes might influence each other's expression levels. To address this question we used the *S. typhimurium* infection model and knocked down *mpeg1* or *mpeg1.2* by injecting morpholinos specific for each gene (supplementary fig. 3A-D). When *mpeg1* was knocked down, the expression of *mpeg1.2* was up-regulated to a lower extent than in the control infected group (fig. 3E). In contrast, when *mpeg1.2* was knocked down the down-regulation of *mpeg1* was unchanged during *S. typhimurium* infection (fig. 3F). Since the *mpeg1* morpholino sequence did not overlap with the sequence of *mpeg1.2*, the *mpeg1* knockdown effect on *mpeg1.2* gene expression is unlikely to be due to a cross-reaction between the *mpeg1* morpholino and the *mpeg1.2* mRNA. Furthermore, we excluded that morpholino treatments might have affected macrophage or neutrophil numbers (supplementary fig. 3E). Therefore, our results suggest that the infection-dependent up-regulation of *mpeg1.2* is partially dependent on the presence of a functional Mpeg1.

The innate immune response is initiated by detection of microbes through pattern recognition receptors, including Toll-like receptors (TLRs), which signal via both Myd88-dependent and Myd88-independent pathways [34]. Our previous analysis of a Myd88-deficient zebrafish mutant showed that a major part of the innate immune response of zebrafish embryos to bacterial infections is dependent on this central TLR signalling adaptor [20]. To determine whether the regulation of *mpeg1* and *mpeg1.2* in response to infection is Myd88–dependent, we injected *S. typhimurium* into *myd88* mutants and their wildtype siblings. Down-regulation of *mpeg1* at 8 hpi was observed in *myd88* mutants similar to the wild type (fig. 4A). In contrast, *mpeg1.2* up-regulation was reduced to approximately 30% of the level observed for wild type infected embryos (fig. 4B). The TLR ligand LPS was sufficient to induce *mpeg1.2* up-regulation (fig. 4C), but did not lead to *mpeg1* down-regulation (data not shown). LPS-mediated up-regulation of *mpeg1.2* was abolished by *myd88* mutation or by inhibition of transcription factor NFκB, which functions downstream of TLR-Myd88 signalling (fig. 4C). In conclusion, up-regulation of *mpeg1.2* expression is partly dependent on MyD88-NFκB signalling, while down-regulation of *mpeg1* appears to be mediated by a Myd88-independent mechanism.

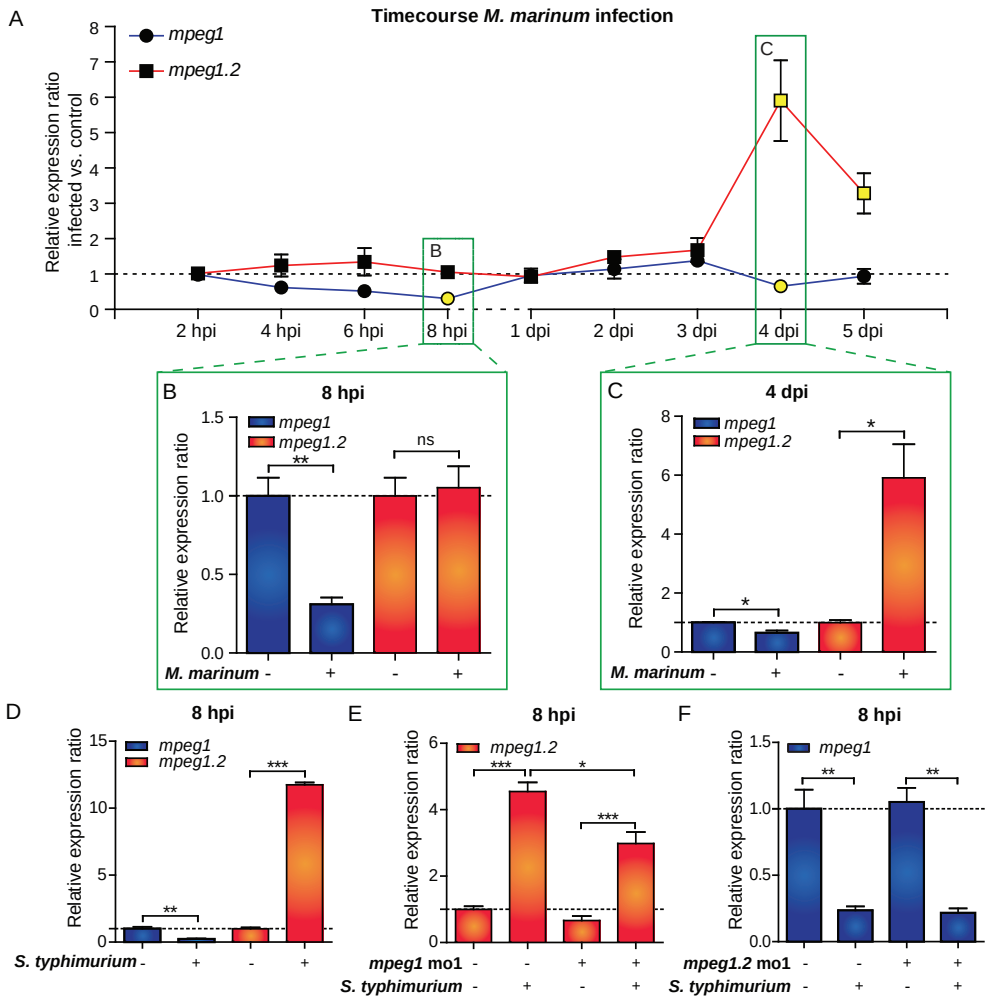

Figure 3. *mpeg1* is down-regulated and *mpeg1.2* is up-regulated upon bacterial infections. (A-C) *mpeg1* and *mpeg1.2* expression during *M. marinum* infection. AB/TL embryos were injected with *M. marinum* Mma20 bacteria (200 cfu) or 2% PVP as a mock control. Expression of *mpeg1* (round data points) and *mpeg1.2* (square data points) was analysed by qPCR at 2, 4, 6 and 8 hpi and at 1, 2, 3, 4 and 5 dpi. Light colouring of the data point in A indicates that expression in infected embryos was significantly different from uninfected controls, and in B and C the full data sets are shown for the time point indicated with boxes in A. (D) *mpeg1* and *mpeg1.2* expression in response to *S. typhimurium* SL1027 infection. AB/TL embryos were injected with 200 cfu of bacteria or mock injected with PBS, and qPCR was performed at 8 hpi. (E, F) Effect of *mpeg1* and *mpeg1.2* morpholino knockdown on each other's gene expression. AB/TL embryos were injected with (F) *mpeg1* or (G) *mpeg1.2* morpholino and subsequently infected with *S. typhimurium* SL1027 as in D. Note that *mpeg1* knockdown had a reducing effect on the up-regulation of *mpeg1.2* expression by *S. typhimurium* infection, while *mpeg1.2* knockdown did not affect the infection-dependent down-regulation of *mpeg1*. Verification of the knockdown effects is shown in supplementary fig. 4A-D. qPCR results are presented as relative ratios of three biological replicates of the infected groups compared to the relevant mock injected control groups (n=18 per group).

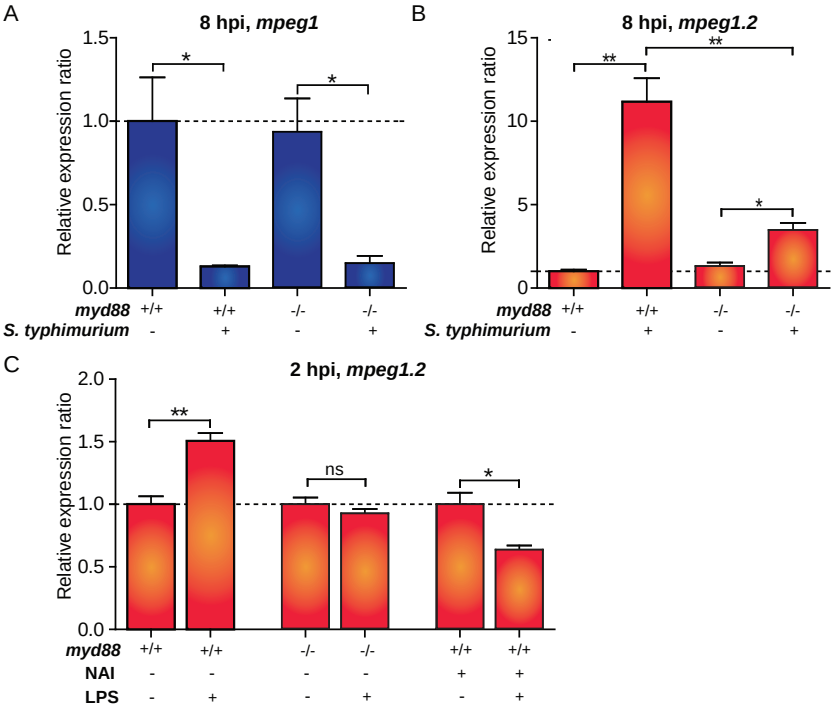

Figure 4. *mpeg1.2* up-regulation but not mpeg1 down-regulation is Myd88 and NFκB dependent. (A-B) Effect of *myd88* mutation on the response of *mpeg1* and *mpeg1.2* to *S. typhimurium* infection. Expression levels of (A) *mpeg1* and (B) *mpeg1.2* were determined by qPCR for *myd88+/+* and *myd88*$^{-/-}$ embryos at 8 hpi after infection with *S. typhimurium* SL1027 bacteria (150 cfu) and mock PBS injected controls; (C) Effect of *myd88* mutation and NFκB inhibition on the response of *mpeg1.2* to LPS treatment. *mpeg1.2* expression in *myd88+/+, myd88*$^{-/-}$ and NFκB activation inhibitor (NAI) treated embryos in response to injection with purified LPS (100 µg/ml) or PBS as a control was determined at 2 hpi. All graphs show data combined from three biological replicates (*n*=20 per group, pooled per replicate).

Knockdown of *mpeg1* leads to impaired control of *M. marinum* infection

To study the function of Mpeg1 and Mpeg1.2 during bacterial infection we used splice morpholinos targeting each gene. First, we investigated the effect of knocking down *mpeg1* on *M. marinum* infection. The morphants and their controls were injected with mCherry-expressing *M. marinum* at 28 hpf and the bacterial fluorescent pixels per embryo were analysed at 4 dpi, when granuloma-like aggregates are formed (fig. 2). *mpeg1* morphants showed higher levels of infection with *M. marinum* compared to their controls (fig. 5A+C). The higher bacterial load in the *mpeg1* morphants was phenocopied with a second morpholino (fig. 5B+D). *M. marinum* infection experiments were terminated at 5 dpi before larvae reached the free-feeding stage and *mpeg1* morphants did not die from the increased bacterial load during this period. We did not expect to see an effect on bacterial load in the *mpeg1.2* morphants since the expression of this gene is barely detectable during the first days of development and only becomes

induced at 4 dpi. As expected, *mpeg1.2* knockdown with two different morpholinos did not have an effect on *M. marinum* infection (fig. 5E-H). While *mpeg1.2* may be important at later larval stages that cannot be analysed by morpholino knockdown, we conclude that only Mpeg1 plays an important role in controlling the early pathogenesis of *M. marinum* infection.

The observation that embryos deficient in Mpeg1 develop increased infection is consistent with the expected anti-bacterial function of Mpeg1 proteins as members of the MACPF superfamily. We next investigated if, other than such a direct anti-bacterial role, Mpeg1 might be important for macrophage functions such as phagocytosis or migration. A phagocytosis assay was performed using both morpholinos targeting *mpeg1*. The morphants and their controls were injected with 180 cfu of mCherry-expressing Mma20 at 30 hpf and these embryos were fixed at the time points 5, 10, 20, 30 and 40 minutes post infection (mpi). Leukocytes were immuno-labelled with L-plastin antibody and Alexa488-conjugated secondary antibody [31] and all intracellular and extracellular Mma20 were counted over the yolk sac of each embryo to determine the percentage of phagocytosis. The yolk sac is an ideal location for analysing phagocytosis due to the superficial position of the blood circulation, which enables easy imaging, and this location is distant from the injection site, thereby minimizing possible wounding effects on the behaviour of macrophages. We observed normal levels of phagocytosis in both *mpeg1* morphants at all stages post infection (fig. 6A), demonstrating that Mpeg1 does not play a role in the phagocytosis of *M. marinum*. Since inflammation plays an important role in *M. marinum*-granuloma environment, we also investigated of *mpeg1* deficiency might have a general effect on leukocyte recruitment. We therefore performed the chemically induced inflammation (ChIN) assay [24] on *mpeg1* morphants and their controls. The copper-induced damage of neuromast hair cells in this assay was capable of attracting both macrophages and neutrophils in the *mpeg1* morphants similar as in the control group (fig. 6B). In summary, Mpeg1 does not affect the basal response of macrophages to infection, such as phagocytosis of *M. marinum*, or migration of leukocytes towards local inflammation sites.

We next sought out to identify whether the *mpeg1* morphants have a differently regulated immune response to *M. marinum.* To this end, we subjected pools of approximately 30 infected and uninfected *mpeg1* morphants to RNA sequencing analysis at 4 dpi and compared the infection response with that of embryos treated with control morpholino. We focused this comparison on a preselected set of 33 genes that showed robust and reproducible up-regulation by *M. marinum* infection at 4 dpi in four independent experiments (supplementary table 2). Approximately one third of the genes in this set, including pro-inflammatory markers such as *il1b*, *mmp9*, and *mmp13a*, showed a similar level of *M. marinum*-induced up-regulation in *mpeg1* morphants as in control embryos (fig. 7A). Other genes showed approximately 2-3-fold higher up-regulation in the *mpeg1* morphant group, including *hamp2*, *hpx*, *steap4*, and genes for a non-coding RNA (*si:dkey-97i18.5*) or uncharacterised proteins

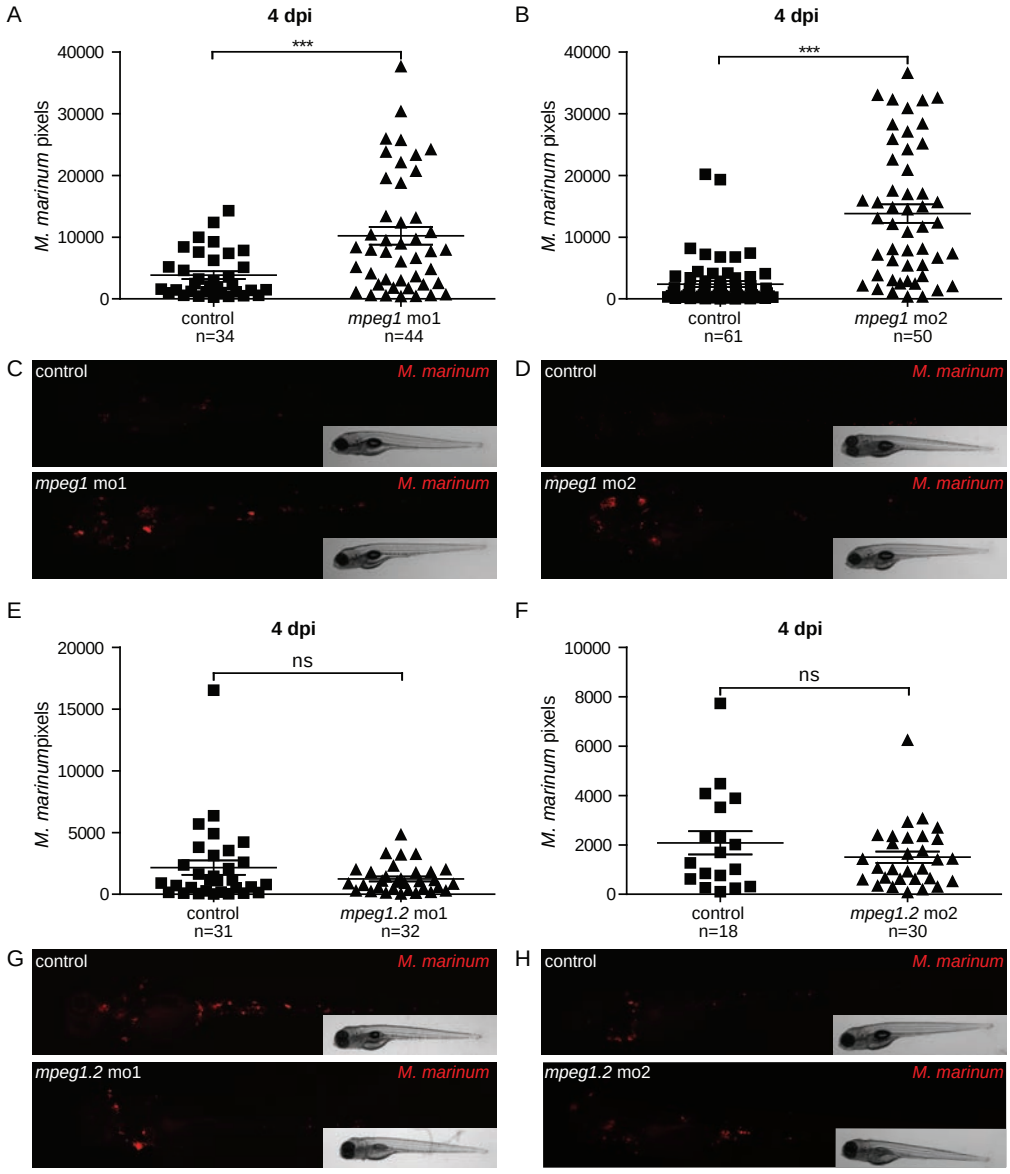

Figure 5. *mpeg1* knockdown impairs control of *M. marinum* infection. AB/TL embryos were injected with two different splice blocking morpholinos against (A-D) *mpeg1* or (E-H) *mpeg1.2* or with control morpholino, subsequently injected with mCherry-expressing *M. marinum* Mma20 strain and infected embryos were imaged at 4 dpi. (A, B, E, F) Bacterial burden was quantified by determining the number of fluorescent bacterial pixels with dedicated software and (C, D, G, H) representative stereo fluorescent images are shown below the graph of each experiment. Graphs show one representative result of five (A) or three (B, E, and F) repeated independent experiments. Each data point represents an individual embryo.

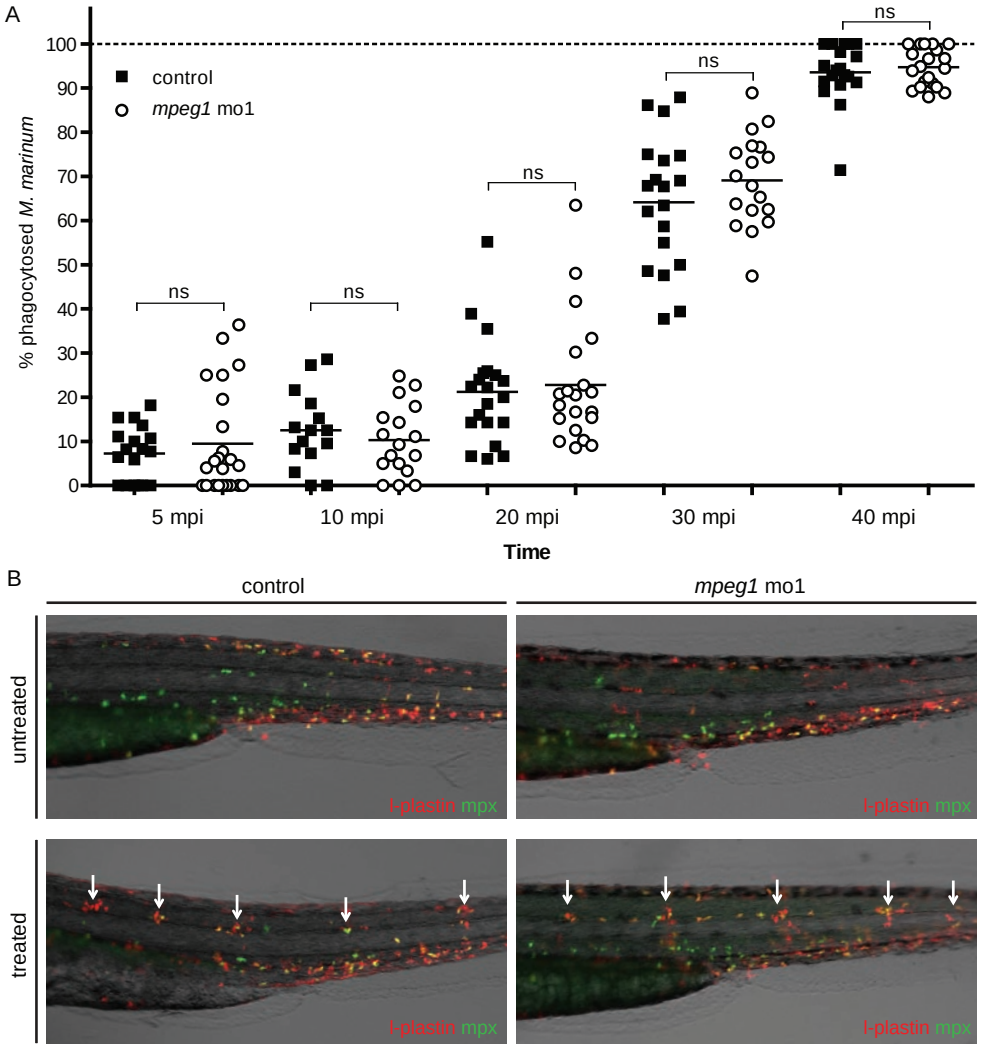

Figure 6. *mpeg1* does not play a role in phagocytosis of *M. marinum* or in leukocyte migration towards local inflammation. (A) Quantification of *M. marinum* phagocytosis. *mpeg1* morphants and their controls were injected with mCherry-expressing *M. marinum* Mma20 strain (180 cfu), fixed at 5, 10, 20, 30 and 40 mpi, and stained with L-plastin Ab to label leukocytes. Intra- and extra-cellular bacteria were counted over the yolk sac and results are presented as percentage of phagocytosed Mma20. (B) Representative images of untreated and copper sulphate treated control and *mpeg1* morphant 3 dpf embryos. Embryos were immuno-labelled with Ab against the general leukocyte marker L-plastin (red signal) in combination with a neutrophil-specific Mpx TSA-staining (green signal). White arrows indicate accumulation of leukocytes at the local inflammation sites at the neuromasts.

(*cabz01040055.1 ct027762.4*). Additionally there was a group of genes with notably lower expression in infected *mpeg1* morphants (less than 28% of the expression level in infected control embryos), which included *cyp24a1*, *hmox1*, *igfbp1a*, *slc25a38a*, and another non-coding RNA gene (*si:ch211-243g18.3*). The effect of *mpeg1* knockdown on the *M. marinum*-induced gene expression profile was markedly different from the effects of two other genes that we analysed for comparison: *ptpn6* and *myd88*. Knockdown of *ptpn6*, previously shown to function as a negative regulator of the innate immune response [23], led to a hyper-induction of approximately two third of the genes in the same gene set, including the inflammatory markers *il1b*, *mmp9*, and *mmp13a* (fig. 7B). In contrast, these inflammatory markers and the majority of other genes in the gene set showed a strongly reduced expression in *M. marinum*-infected *myd88* mutants (fig. 7C), consistent with the function of MyD88 protein as an adaptor in Toll-like and Interleukin receptor signalling [20]. We have previously shown that both the hyper-induced immune response in *ptpn6* morphants and the immunodeficiency of *myd88* mutants are associated with an increased susceptibility to *M. marinum* [20, 23]. Since the *mpeg1* knockdown effect on the *M. marinum*-dependent gene set is clearly different from both phenotypes, there is no indication that a general hyper-induction of the immune response or a general immunodeficiency could be the underlying cause of the increased bacterial burden under *mpeg1* knockdown conditions.

Mpeg1 and Mpeg1.2 both function in controlling *S. typhimurium* infection

As described above, the more acute phenotype of *S. typhimurium* infection led to rapid up-regulation of *mpeg1.2* gene expression, while *mpeg1* was simultaneously down-regulated (fig. 4A-B). To determine whether Mpeg1 and Mpeg1.2 play an anti-bacterial role during this acute infection, we injected *S. typhimurium* in *mpeg1* and *mpeg1.2* morphants at 28 hpf and assessed bacterial burden by cfu counts. Plating embryos for cfu counts showed that at 1 hpi all groups started with equal levels of *S. typhimurium* and that at 16 hpi morphants of *mpeg1* and *mpeg1.2* both had approximately 6-fold higher cfu counts than the control group (fig. 8A). Increased cfu counts were also observed with a second set of morpholinos for *mpeg1* and *mpeg1.2* (fig. 8B). This striking difference in the cfu counts indicates that both genes play a role in controlling the *S. typhimurium* infection in zebrafish embryos.

Next, we aimed to determine whether the higher cfu numbers in the morphants was associated with a decreased survival rate. Morphants of *mpeg1* and *mpeg1.2* and control embryos were injected with *S. typhimurium*, screened for equal level of infection under a stereo fluorescence microscope directly after injection, and monitored for heart beat from 14 hpi onwards. *mpeg1.2* deficiency caused a similar or decreased survival time compared to the control group (fig. 8C-D) and unexpectedly, *mpeg1* morphants survived significantly longer than the control embryos (fig. 8C-D), despite that these morphants showed increased cfu counts similar to *mpeg1.2* morphants. This opposing effect on survival could not be attributed to a difference in intracellular or extracellular location of *S. typhimurium* between the two morphants because both

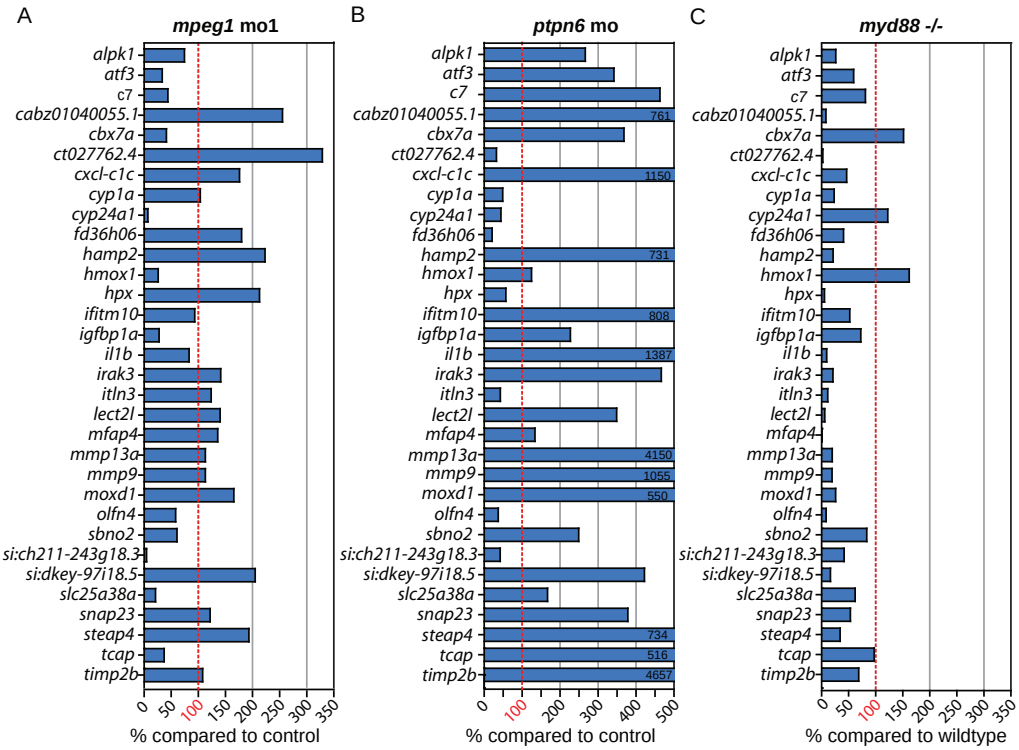

Figure 7. Effect of *mpeg1* knockdown on the innate immune response during *M. marinum* infection in comparison with known effects of *ptpn6* and *myd88* deficiencies. Graphs show the effects of (A) *mpeg1* mo1 knockdown, (B) *ptpn6* morpholino knockdown and (C) *myd88* mutation on a set of genes that showed reproducible induction by *M. marinum* infection in control embryos. The expression level of these genes under conditions of *mpeg1*, *ptpn6* or *myd88* deficiency is expressed as the percentage of the expression level in the corresponding control. Results are based on RNAseq analysis of pools of 30 infected and 30 uninfected embryos for each group. Embryos were injected with *M. marinum* Mma20 (300 cfu) or mock injected with 2% PVP, and RNAseq analysis was performed at 4 dpi.

Figure 8. *mpeg1* and *mpeg1.2* knockdown increase bacterial burden and pro-inflammatory gene expression, but have opposite effects on host survival during *S. typhimurium* infection. (A-B) Quantification of bacterial burden. *mpeg1* and *mpeg1.2* morphants ((A) morpholinos 1 and (B) morpholinos 2) and control embryos were injected with Ds-Red-expressing *S. typhimurium* SL1027 bacteria (200 cfu) and PBS as mock control. Embryos were homogenised and plated at 1 and 16 hpi to determine *S. typhimurium* cfu counts (n=5 per group, 2 biological replicates, log2 scale). (C-D) Survival rates. The percentage of survival of infected *mpeg1* morphants, *mpeg1.2* morphants ((C) morpholinos 1 and (D) morpholinos 2) and control embryos was determined over a time course of 32 hpi. DsRed-expressing *S. typhimurium* SL1027 bacteria were injected into the blood circulation (150 cfu). Survival curves of *mpeg1* morphants (red line), *mpeg1.2* morphants (green line) and control embryos (blue line) are shown of one representative experiment of three individual experiments. (E) Quantification of intracellular and extracellular *S. typhimurium* over the Duct of Cuvier in control embryos, *mpeg1* morphants and *mpeg1.2* morphants at 4 and 8 hpi (representative confocal images in supplementary fig.4). Statistical significance is indicated for intracellular *S. typhimurium* (red letters) and extracellular *S. typhimurium* (blue letters) (calculated from confocal images of n=6-8 embryos per group).

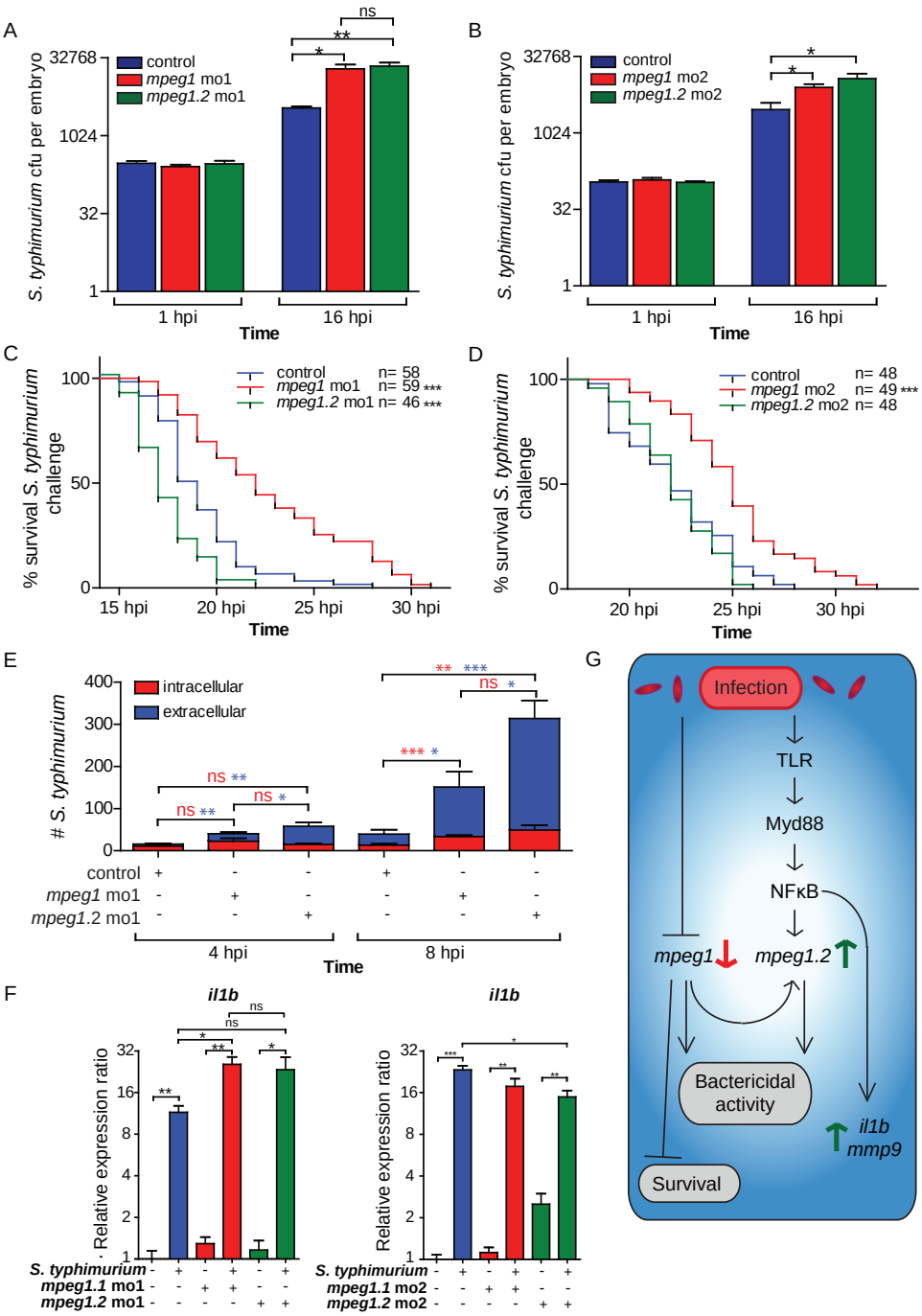

Figure 8 continued: (F) Pro-inflammatory gene expression of *il1b* under the same experimental conditions as in A-B was analysed by qPCR at 16 hpi (*n*=15 per group, pooled per replicate, 3 biological replicates, log2 scale). (G) A schematic representation of *mpeg1* and *mpeg1.2* regulation and their function.

mpeg1 and *mpeg1.2* morphants showed a significantly higher number of extracellular *S. typhimurium* compared to the control embryos at 8 hpi (fig. 8E and supplementary fig. 4). Furthermore, the opposing survival effect could also not be attributed to a difference in expression of the major *S. typhimurium* responsive pro-inflammatory genes, *il1b* (fig. 8F) and *mmp9* (supplementary fig. 5), which showed clear induction in *mpeg1* and *mpeg1.2* morphants. While the increased survival rate of *mpeg1* morphants remains unexplained, our results suggest that the up-regulation of *mpeg1.2* with concomitant down-regulation of *mpeg1* aids the host in combatting *S. typhimurium* infection (fig. 8G).

Discussion

The perforins of cytotoxic T-cells and natural killer cells and the membrane attack complex proteins of the complement system share the ability to form pores in membranes [1, 2]. While the roles of these proteins in host defence are well understood, the function of the structurally related MPEG1/Perforin-2 family in macrophages remains to be fully elucidated [3, 9]. In zebrafish an *mpeg1*-expressing population of macrophages develops during the first day of embryogenesis [13]. The availability of well-established infection models for zebrafish embryos enabled us to study the function of *mpeg1* in innate host defence. We show that *mpeg1* is down-regulated during infection in a Myd88-independent manner, while a close homolog, *mpeg1.2*, is up-regulated partially by a Myd88-NFκB-dependent mechanism. Notwithstanding this opposite regulation pattern, we found that both *mpeg1* and *mpeg1.2* are important for controlling infections with intracellular bacterial pathogens.

The close chromosomal location of the different *mpeg1* genes in zebrafish suggests that these are the result of recent gene duplication events, after which *mpeg1* and *mpeg1.2* appear to have developed specialised functions and *mpeg1.3* may have become a pseudogene. A similar situation is found in mice and other rodents, where a gene named pore forming protein-like (*Pfpl*) is most likely paralogous to *Mpeg1*, since it is located in close vicinity and encodes a protein with 66% amino acid identity. Whereas *Mpeg1* is inducible by infection both in macrophages and other cell types [11, 12] the expression pattern of *Pfpl* in trophoblasts indicates a developmental function of this gene [35] and EST profiles in the NCBI database provide no indication for significant expression of *Pfpl* in cells or organs related to the immune system. EST profiles of the single *MPEG1* gene in human support its possible function in the immune system, but to the best of our knowledge, functional studies of the human gene have not yet been reported. Studies of murine *Mpeg1* in cultured fibroblasts, macrophages, and HeLa cells led to the hypothesis that upon bacterial infection Mpeg1/Perforin-2 vesicles traffic to and fuse with bacteria-containing compartments, where attack and pore formation on the bacterial surface is subsequently initiated [3, 11, 12]. To further investigate the correlation of *MPEG1* with infectious diseases, we inspected curated microarray datasets in the NextBio database (http://www.nextbio.com/b/nextbioCorp.nb). This analysis shows

that *MPEG1* is frequently regulated during infection, both in studies using cultured macrophages and in studies using mouse infection models. For example, *MPEG1* shows significant down-regulation in human macrophages exposed to *Staphylococcus aureus* [36] and in human monocytes infected with *Francisella tularensis* [37]. In contrast, up-regulation has been observed in for example the lungs of mice infected with these pathogens [38, 39]. Thus, in human and mouse different infection conditions are associated either with up- or down-regulation of *MPEG1,* while in zebrafish *mpeg1* and *mpeg1.2* are regulated in opposite directions under the same infection conditions.

Using the zebrafish-*M. marinum* infection model we found that knockdown of *mpeg1* results in increased bacterial burden, consistent with the proposed bactericidal function of Mpeg1 as a pore forming molecule [11]. However, there might be a broader effect as we observed an altered immune response expression signature in infected *mpeg1* morphants that might also have an impact on the ability to control infection. The function of *mpeg1.2*, which has extremely low basal expression level, could only be assessed using an *S. typhimurium* infection model, where this gene is rapidly up-regulated. In this model, knockdown of *mpeg1* attenuated the up-regulation of *mpeg1.2*, indicating a broader effect of *mpeg1* on the innate immune response consistent with the results of *M. marinum* infection. Knockdown of either *mpeg1* or the inducible *mpeg1*.2 gene led to increased bacterial burden of *S. typhimurium* infection, providing *in vivo* support for the anti-bacterial function of both genes. Due to toxicity effects of combining the morpholinos we were unable to investigate possible synergism between the anti-bacterial functions of *mpeg1* and *mpeg1.2*. However, a remarkable difference between the separate knockdown of *mpeg1* and *mpeg1.2* was observed in that the survival time of *mpeg1* morphants was prolonged despite the increase in cfu numbers. This suggests that the survival advantage of *mpeg1* morphants could be due to an altered immune response and that, during the normal course of *S. typhimurium* infection, embryos might die from host damaging effects of the immune response rather than as a direct effect of the bacterial load. That *S. typhimurium*-infected zebrafish embryos die primarily from a host damaging immune response is supported by our previous study of the regulatory phosphatase Ptpn6. Deficiency in Ptpn6 leads to a decreased survival rate during *S. typhimurium* infection, which correlates with a hyper-induced expression of many pro-inflammatory genes [23]. Two of the main pro-inflammatory marker genes, *il1b* and *mmp9*, were highly up-regulated in both *mpeg1* and *mpeg1.2* morphants, similar to infected control embryos. A difference in the expression of these marker genes therefore does not explain the survival advantage of *mpeg1* morphants and the underlying cause of this effect currently remains unknown. Together, this first study of the MPEG1/Perforin-2 family in a whole organism model enables us to present a scheme that summarises the regulatory mechanisms of both *mpeg1* and *mpeg1.2* and links this to the biological effects of the two genes (fig. 8G). The specialised function of the two *mpeg1* paralogues in zebrafish indicated by our morpholino knockdown study can be seen as a motivation to develop zebrafish or mouse knockout models for further investigation of the mechanisms by which Mpeg1/Perforin-2 proteins exert their immunological function.

Acknowledgements

The authors would like to thank Georges Lutfalla (University Montpellier 2) for the kind gift of *Tg(mpeg1:mCherry-F)* fish, Michiel van der Vaart for providing RNA of LPS injected myd88 mutant embryos, Ulrike Nehrdich, Laura van Hulst and Davy de Witt for fish care, and other lab members for helpful discussions. EB, AEN, FJV, HPS, and AHM were supported by the Smart Mix Program of the Netherlands Ministry of Economic Affairs and the Ministry of Education, Culture and Science, PIR by a Marie Curie Intra-European Fellowship (PIEF-GA-2010-274389), and JR by a Marie Curie Fellowship of the European 7th Framework Initial Training Network FishForPharma (PITG-GA-2011-289209).

References

1. Kondos, S.C. et al. The structure and function of mammalian membrane-attack complex/perforin-like proteins. Tissue Antigens 76, 341-351 (2010).

2. Rosado, C.J. et al. The MACPF/CDC family of pore-forming toxins. Cell Microbiol 10, 1765-1774 (2008).

3. McCormack, R., de Armas, L., Shiratsuchi, M. & Podack, E.R. Killing machines: three pore-forming proteins of the immune system. Immunol Res 57, 268-278 (2013).

4. Voskoboinik, I., Dunstone, M.A., Baran, K., Whisstock, J.C. & Trapani, J.A. Perforin: structure, function, and role in human immunopathology. Immunol Rev 235, 35-54 (2010).

5. Spilsbury, K. et al. Isolation of a novel macrophage-specific gene by differential cDNA analysis. Blood 85, 1620-1629 (1995).

6. Wiens, M. Innate Immune Defense of the Sponge Suberites domuncula against Bacteria Involves a MyD88-dependent Signaling Pathway: INDUCTION OF A PERFORIN-LIKE MOLECULE. Journal of Biological Chemistry 280, 27949-27959 (2005).

7. Renault, T., Faury, N., Barbosa-Solomieu, V. & Moreau, K. Suppression substractive hybridisation (SSH) and real time PCR reveal differential gene expression in the Pacific cupped oyster, Crassostrea gigas, challenged with Ostreid herpesvirus 1. Dev Comp Immunol 35, 725-735 (2011).

8. Kemp, I.K. & Coyne, V.E. Identification and characterisation of the Mpeg1 homologue in the South African abalone, Haliotis midae. Fish & Shellfish Immunology 31, 754-764 (2011).

9. D'Angelo, M.E., Dunstone, M.A., Whisstock, J.C., Trapani, J.A. & Bird, P.I. Perforin evolved from a gene duplication of MPEG1, followed by a complex pattern of gene gain and loss within Euteleostomi. BMC Evol Biol 12, 59 (2012).

10. Kopacek, J. et al. Upregulation of the genes encoding lysosomal hydrolases, a perforin-like protein, and peroxidases in the brains of mice affected with an experimental prion disease. J Virol 74, 411-417 (2000).

11. McCormack, R., de Armas, L.R., Shiratsuchi, M., Ramos, J.E. & Podack, E.R. Inhibition of intracellular bacterial replication in fibroblasts is dependent on the perforin-like protein (perforin-2) encoded by macrophage-expressed gene 1. J Innate Immun 5, 185-194 (2013).

12. Fields, K.A., McCormack, R., de Armas, L.R. & Podack, E.R. Perforin-2 restricts growth of Chlamydia trachomatis in macrophages. Infect Immun 81, 3045-3054 (2013).

13. Zakrzewska, A. et al. Macrophage-specific gene functions in Spi1-directed innate immunity. Blood 116, e1-11 (2010).

14. Ellett, F., Pase, L., Hayman, J.W., Andrianopoulos, A. & Lieschke, G.J. mpeg1 promoter transgenes direct macrophage-lineage expression in zebrafish. Blood 117, e49-e56 (2010).

15. Herbomel, P., Thisse, B. & Thisse, C. Ontogeny and behaviour of early macrophages in the zebrafish embryo. Development 126, 3735-3745 (1999).

16. Trede, N.S., Langenau, D.M., Traver, D., Look, A.T. & Zon, L.I. The use of zebrafish to understand immunity. Immunity 20, 367-379 (2004).

17. Davis, J.M. et al. Real-time visualization of mycobacterium-macrophage interactions leading to initiation of granuloma formation in zebrafish embryos. Immunity 17, 693-702 (2002).

18. van der Sar, A.M. et al. Zebrafish embryos as a model host for the real time analysis of Salmonella typhimurium infections. Cellular Microbiology 5, 601-611 (2003).

19. Meijer, A.H. & Spaink, H.P. Host-pathogen interactions made transparent with the zebrafish model. Curr Drug Targets 12, 1000-1017 (2011).

20. van der Vaart, M., van Soest, J.J., Spaink, H.P. & Meijer, A.H. Functional analysis of a zebrafish myd88 mutant identifies key transcriptional components of the innate immune system. Dis Model Mech 6, 841-854 (2013).

21. Renshaw, S.A. et al. A transgenic zebrafish model of neutrophilic inflammation. Blood 108, 3976-3978 (2006).

22. Bernuta, A. et al. Mycobacterium abscessus cording prevents phagocytosis and promotes abscess formation. PNAS in press (2014).

23. Kanwal, Z. et al. Deficiency in hematopoietic phosphatase ptpn6/Shp1 hyperactivates the innate immune system and impairs control of bacterial infections in zebrafish embryos. J Immunol 190, 1631-1645 (2013).

24. d'Alençon, C.A. et al. A high-throughput chemically induced inflammation assay in zebrafish. BMC Biology 8, 151 (2010).

25. van der Sar, A.M. et al. Mycobacterium marinum Strains Can Be Divided into Two Distinct Types Based on Genetic Diversity and Virulence. Infection and Immunity 72, 6306-6312 (2004).

26. Cosma, C.L., Humbert, O., Sherman, D.R. & Ramakrishnan, L. Trafficking of superinfecting Mycobacterium organisms into established granulomas occurs in mammals and is independent of the Erp and ESX-1 mycobacterial virulence loci. J Infect Dis 198, 1851-1855 (2008).

27. Veneman, W.J. et al. A zebrafish high throughput screening system used for Staphylococcus epidermidis infection marker discovery. BMC Genomics 14, 255 (2013).

28. Benard, E.L. et al. Infection of zebrafish embryos with intracellular bacterial pathogens. J Vis Exp pii: 3781. doi: 10.3791/3781 (2012).

29. Stockhammer, O.W., Zakrzewska, A., Hegedus, Z., Spaink, H.P. & Meijer, A.H. Transcriptome profiling and functional analyses of the zebrafish embryonic innate immune response to Salmonella infection. J Immunol 182, 5641-5653 (2009).

30. Meijer, A.H. et al. Identification and real-time imaging of a myc-expressing neutrophil population involved in inflammation and mycobacterial granuloma formation in zebrafish. Developmental and comparative immunology 32, 36-49 (2008).

31. Mathias, J.R. et al. Live imaging of chronic inflammation caused by mutation of zebrafish Hai1. Journal of Cell Science 120, 3372-3383 (2007).

32. Nezhinsky A.E., V.F.J. Efficient and Robust Shape Retrieval from Deformable Templates. International Symposium on Leveraging Applications of Formal Methods Part II, LNCS 7610 (T. Margaria, B. Steffen, and M. Merten (Eds.)), 42-55 (2012).

33. Clay, H., Volkman, H.E. & Ramakrishnan, L. Tumor Necrosis Factor Signaling Mediates Resistance to Mycobacteria by Inhibiting Bacterial Growth and Macrophage Death. Immunity 29, 283-294 (2008).

34. O'Neill, L.A. & Bowie, A.G. The family of five: TIR-domain-containing adaptors in Toll-like receptor signalling. Nat Rev Immunol 7, 353-364 (2007).

35. Hemberger, M., Himmelbauer, H., Ruschmann, J., Zeitz, C. & Fundele, R. cDNA subtraction cloning reveals novel genes whose temporal and spatial expression indicates association with trophoblast invasion. Dev Biol 222, 158-169 (2000).

36. Koziel, J. et al. Phagocytosis of Staphylococcus aureus by macrophages exerts cytoprotective effects manifested by the upregulation of antiapoptotic factors. PLoS One 4, e5210 (2009).

37. Butchar, J.P. et al. Microarray analysis of human monocytes infected with Francisella tularensis identifies new targets of host response subversion. PLoS One 3, e2924 (2008).

38. Frank, K.M. et al. Host response signature to Staphylococcus aureus alpha-hemolysin implicates pulmonary Th17 response. Infection and immunity 80, 3161-3169 (2012).

39. Walters, K.A. et al. Francisella tularensis subsp. tularensis induces a unique pulmonary inflammatory response: role of bacterial gene expression in temporal regulation of host defense responses. PLoS One 8, e62412 (2013).

40. Volkman, H.E. et al. Tuberculous granuloma formation is enhanced by a mycobacterium virulence determinant. PLoS Biol 2, e367 (2004).

A Protein homology

Similar \ Identical	z-Mpeg1	z-Mpeg1.2	z-Mpeg1.3	m-MPEG1	h-MPEG1
z-Mpeg1	100	66	69	45	48
z-Mpeg1.2	89	100	56	44	46
z-Mpeg1.3	85	81	100	43	43
m-MPEG1	77	74	75	100	75
h-MPEG1	75	73	73	91	100

B MACPF domain homology

Similar \ Identical	z-Mpeg1	z-Mpeg1.2	z-Mpeg1.3	m-MPEG1	h-MPEG1
z-Mpeg1	100	72	70	45	50
z-Mpeg1.2	92	100	59	45	47
z-Mpeg1.3	83	82	100	49	50
m-MPEG1	78	74	84	100	77
h-MPEG1	74	74	82	93	100

Supplementary table 1. Homology between zebrafish Mpeg1 proteins, murine MPEG1 and human MPEG1. Homology for (A) whole protein sequences and (B) MACPF domains was determined between zebrafish Mpeg1 (z-Mpeg1, NP_997902.1), Mpeg1.2 (z-Mpeg1.2, ENSDARP00000063271), Mpeg1.3 (z-Mpeg1.3, ENSDARP00000098563), murine MPEG1 (m-MPEG1, NP_034951.1) and human MPEG1 (h-MPEG1, NP_001034485.1). Amino acid identity and similarity percentages were determined using UniProt CLUSTAL O(1.2.0) multiple sequence alignment.

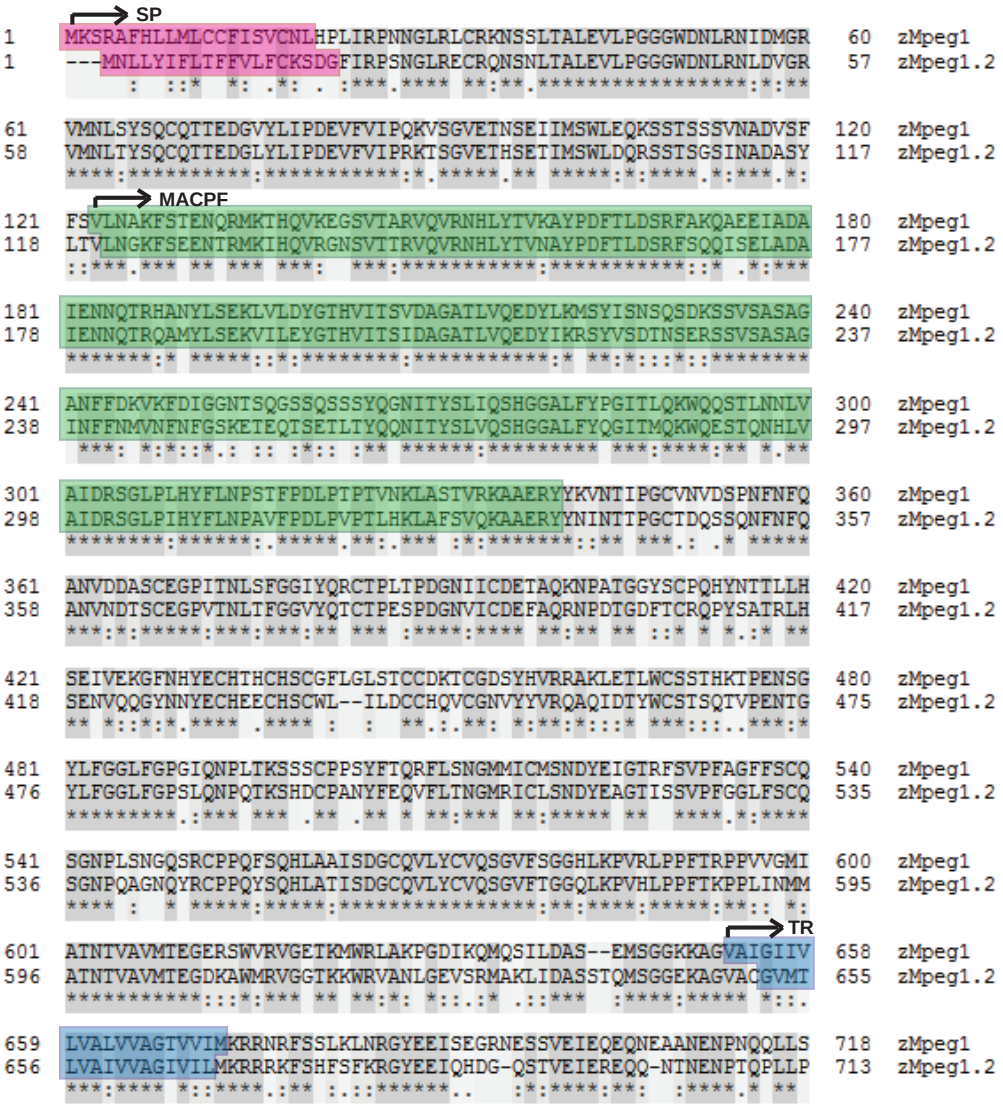

Supplementary figure 1. Mpeg1 and Mpeg1.2 protein alignment. The Signal Peptide (SP), Membrane Attack Complex/Perforin (MACPF), and Transmembrane Region (TR) are located in the same position in Mpeg1 and Mpeg1.2.

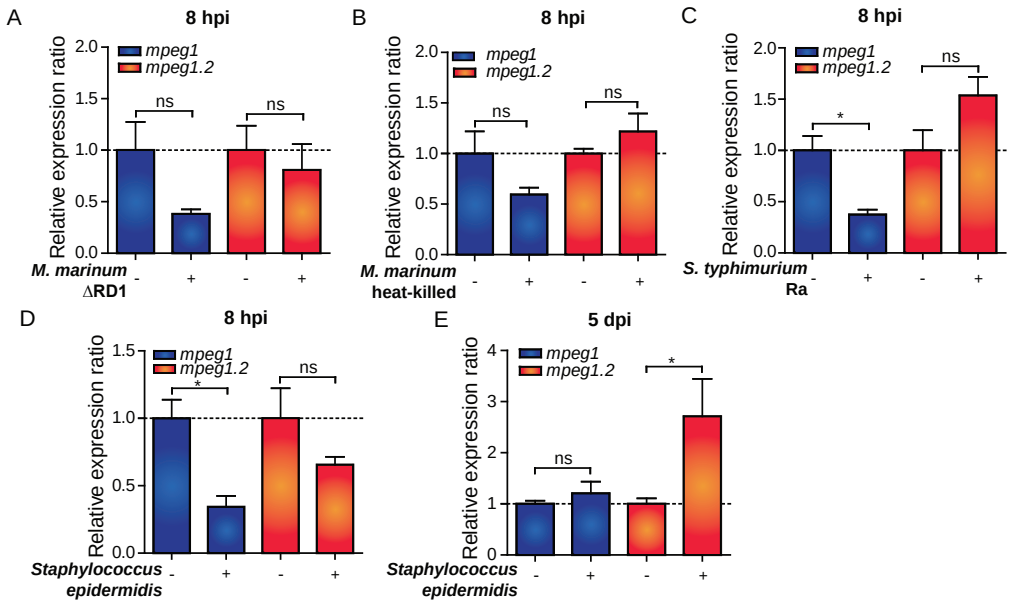

Supplementary figure 2. Expression analysis of *mpeg1* and *mpeg1.2* during different bacterial infections. Expression at 8 hpi following intravenous infection with (A) *M. marinum ΔRD1* [40] (800 cfu), (B) heat-killed *M. marinum* (300 cfu), (C) *S. typhimurium* LPS mutant strain Ra (200 cfu), and (D) *Staphylococcus epidermidis* strain O-47 (800 cfu). (E) Expression at 5 dpi following yolk infection at 2 hpf with *Staphylococcus epidermidis* strain O-47 (20 cfu). Expression levels of *mpeg1* and *mpeg1.2* were determined by qPCR. All graphs show data combined from three biological replicates (*n*=20 per group, pooled per replicate).

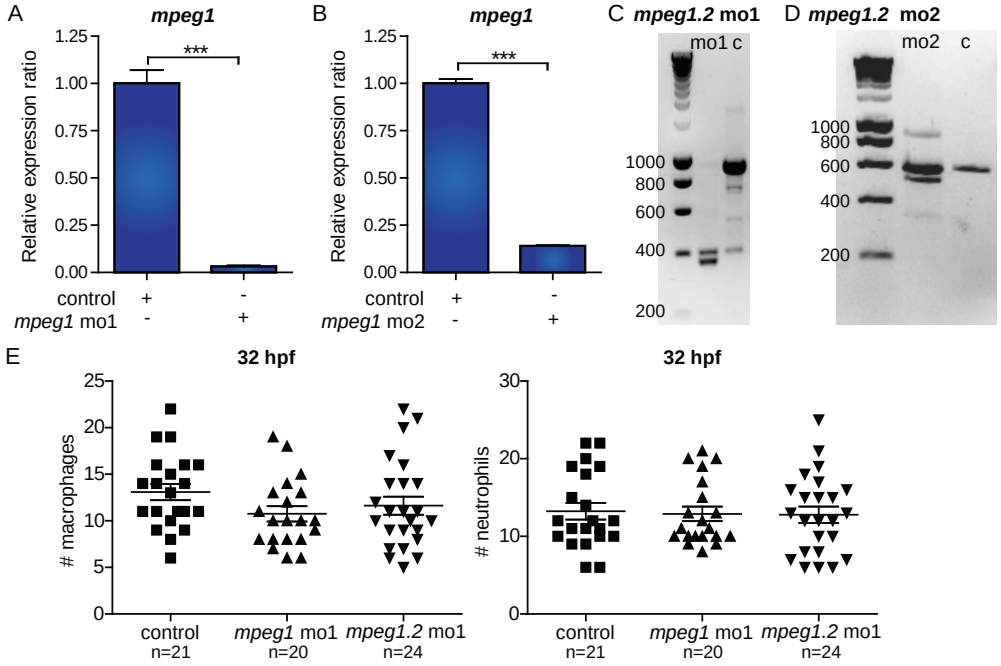

Supplementary figure 3. Verification of *mpeg1* and *mpeg1.2* knockdown. (A-B) Knockdown of *mpeg1*. Expression of *mpeg1* was determined by qPCR at 28 hpf after knockdown with (A) *mpeg1* morpholino 1 (B) *mpeg1* morpholino 2 and in embryos injected with control morpholino. Both forward and reverse qPCR primers target exon 2 of *mpeg1*.(C-D) Knockdown of *mpeg1.2*. Because of the low basal expression level of *mpeg1.2*, the knockdown effect on this gene was assessed under infection conditions (8 hpi). Expression of *mpeg1.2* was determined by RT-PCR using RNA from embryos injected with (C) *mpeg1.2* morpholino 1 (mo1) or control morpholino (c) (D) *mpeg1.2* morpholino 2 (mo2) or control morpholino (c) and infected with *S. typhimurium.* Digits in C and D indicate smart ladder base pair size. For both *mpeg1.2* morphants, the RT-PCR product (944 bp for mo1 and 569 bp in size for mo2) is disrupted upon morpholino injection. The RT-PCR forward primer for *mpeg1.2* targets exon 1 and both RT-PCR reverse primers for *mpeg1.2* target exon 2. (E) Normal leukocyte numbers in *mpeg1* and *mpeg1.2* morphants. *mpeg1* and *mpeg1.2* morphants and control embryos were fixed at 32 hpf and were stained with the neutrophil mpx-TSA staining and immuno-labelled with Ab against the general leukocyte marker L-plastin. Macrophage (L-plastin-positive, mpx negative) and neutrophil (L-plastin/mpx double positive) numbers were counted blinded in the tail (ns = not significant).

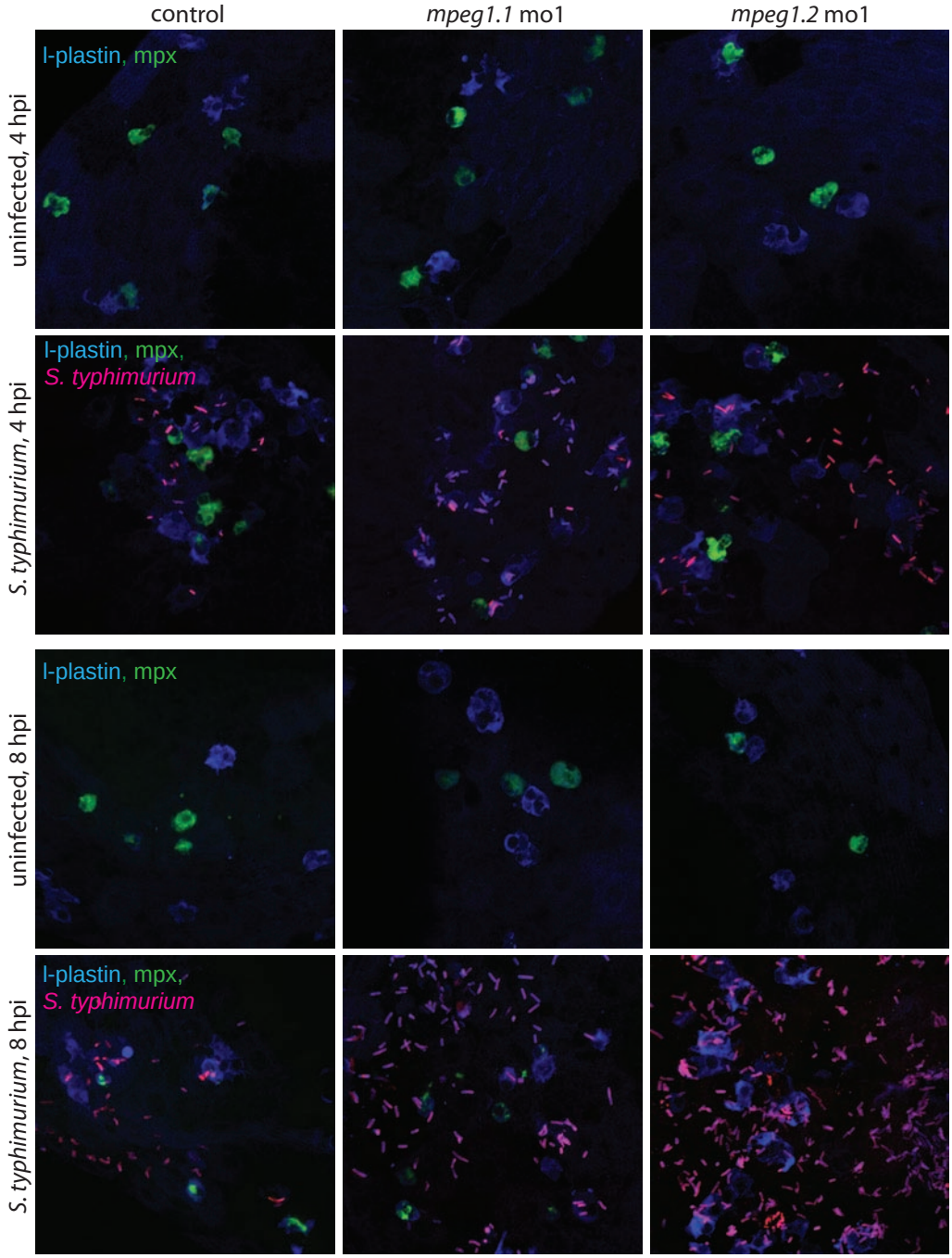

Supplementary figure 4. Representative images of the *S. typhimurium* infection process during *mpeg1* and *mpeg1.2* knockdown. *S. typhimurium* SL1027 bacteria (150 cfu) were injected into the caudal vein of AB/TL embryos. Embryos were fixed at 4 and 8 hpi and stained for mpx activity in neutrophils (green) followed by double antibody staining against *S. typhimurium* (red) and L-plastin (blue). Macrophages are identified as L-plastin-positive, mpx-negative cells

Supplementary figure 4 continued: and no differences in macrophage numbers were observed between the different groups. Confocal z-stack projections show identical locations in the Duct of Cuvier in uninfected and infected control embryos, *mpeg1* (mo1) morphants, and *mpeg1.2* (mo1) morphants. Numbers of *S. typhimurium* bacteria contained within macrophages or extracellular were quantified from images of 6-8 embryos per group and data are shown in Fig. 8E.

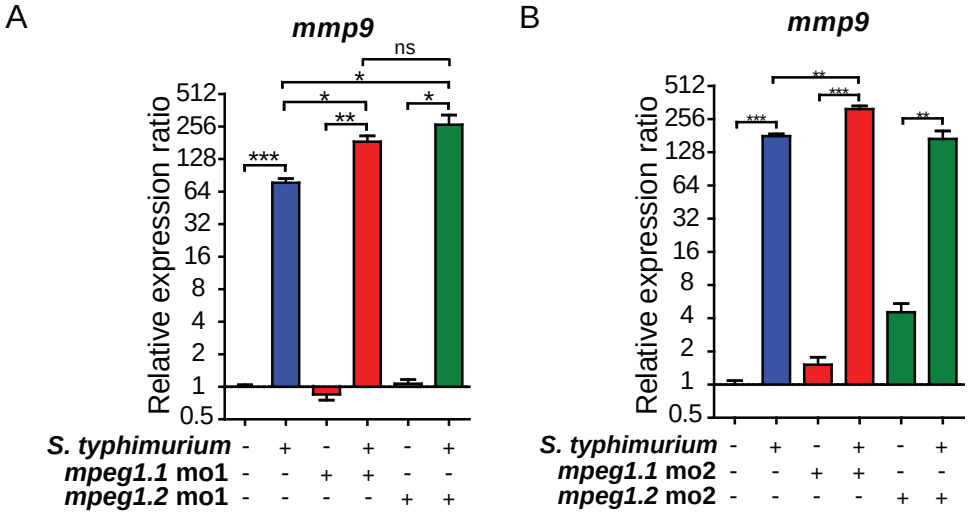

Supplementary figure 5. Expression of *mmp9* during *S. typhimurium* infection of *mpeg1* and *mpeg1.2* knockdown embryos. (A-B) Gene expression of *mmp9* under the same experimental conditions as in fig. 8A-B were analysed by qPCR at 16 hpi (*n*=15 per group, pooled per replicate, 3 biological replicates, log2 scale).

Supplementary table 2. Overview top induced genes *M. marinum* infection.

Ensembl ID	Gene name	Description	log2 fold change	Adjusted P-value
ENSDARG00000059741	*alpk1*	alpha-kinase 1	1.2	4.8E-04
ENSDARG00000007823	*atf3*	activating transcription factor 3	1.7	1.4E-08
ENSDARG00000057121	*c7 (2 of 2)*	complement component 7	1.7	2.0E-06
ENSDARG00000086869	*cabz01040055.1*	three-finger protein 5 (LOC100003647 precursor)	3.1	3.1E-22
ENSDARG00000038025	*cbx7a*	chromobox homolog 7a	1.8	3.9E-10
ENSDARG00000086654	*ct027762.4*	Uncharacterized protein	2.1	5.1E-07
ENSDARG00000075045	*cxcl-c1c*	chemokine (C-X-C motif) ligand c1c	1.7	5.6E-04
ENSDARG00000026039	*cyp1a*	cytochrome P450, family 1, subfamily A	2.5	3.3E-17
ENSDARG00000070420	*cyp24a1*	cytochrome P450, family 24, subfamily A, polypeptide 1	2.2	5.0E-14
ENSDARG00000092858	*fd36h06*	non-coding RNA	2.4	2.2E-10
ENSDARG00000053227	*hamp2*	hepcidin antimicrobial peptide 2	3.0	1.3E-12
ENSDARG00000027529	*hmox1*	heme oxygenase (decycling) 1	1.5	1.9E-04
ENSDARG00000051912	*hpx (1 of 2)*	hemopexin	2.2	1.2E-12
ENSDARG00000093303	*ifitm10*	interferon induced transmembrane protein 10	1.4	1.5E-03
ENSDARG00000014947	*igfbp1a*	insulin-like growth factor binding protein 1a	1.9	1.1E-10
ENSDARG00000005419	*il1b*	interleukin 1, beta	2.4	1.2E-07
ENSDARG00000053131	*irak3*	interleukin-1 receptor-associated kinase 3	2.6	3.0E-08
ENSDARG00000003523	*itln3*	intelectin 3	3.3	3.6E-24
ENSDARG00000033227	*lect2l*	leukocyte cell-derived chemotaxin 2 like	2.3	1.3E-14
ENSDARG00000090557	*mfap4 (6 of 13)*	microfibrillar-associated protein 4	1.9	2.5E-06
ENSDARG00000012395	*mmp13a*	matrix metalloproteinase 13a	2.0	2.8E-09
ENSDARG00000042816	*mmp9*	matrix metalloproteinase 9	2.7	1.6E-23
ENSDARG00000031136	*moxd1*	monooxygenase, DBH-like 1	1.6	3.3E-06
ENSDARG00000074322	*olfn4 (3 of 8)*	olfactomedin 4	1.5	6.0E-04
ENSDARG00000016188	*sbno2 (2 of 3)*	strawberry notch homolog 2 (Drosophila)	1.3	6.6E-05
ENSDARG00000092826	*si:ch211-243g18.3*	non-coding RNA	4.3	3.7E-06
ENSDARG00000090352	*si:dkey-97i18.5*	non-coding RNA	2.4	2.4E-16
ENSDARG00000059805	*slc25a38a*	solute carrier family 25, member 38a	2.0	1.2E-04
ENSDARG00000055252	*snap23 (2 of 2)*	synaptosomal-associated protein, 23kDa	1.6	7.6E-04
ENSDARG00000055901	*steap4*	steap family member 4	1.4	5.8E-05
ENSDARG00000007344	*tcap*	titin-cap (telethonin)	2.2	1.2E-13
ENSDARG00000075261	*timp2b*	tissue inhibitor of metalloproteinase 2b	1.4	4.9E-05

* List of 33 genes that consistently showed significant up-regulation during *M. marinum* infection in at least three out of four independent experiments (adjusted P-value <0.01). AB/TL embryos were injected with control morpholino, subsequently injected with mCherry-expressing *M. marinum* Mma20 strain, and infected embryos and uninfected controls were subjected to RNAseq analysis at 4 dpi.